# Design of solid lipid nanoparticles for skin photoprotection through the topical delivery of caffeic acid-phtalimide

Bruna Terra Alves da Silva, Sueli de Oliveira Silva Lautenschlager, Celso Vataru Nakamura, Valdecir Farias Ximenes, Yu Ogawa, Raphaël Michel, Rachel Auzély-Velty

International Journal of Pharmaceutics 669 (2025) 125010

Contents lists available at ScienceDirect

International Journal of Pharmaceutics

journal homepage: www.elsevier.com/locate/ijpharm

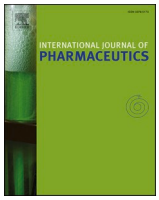

# Design of solid lipid nanoparticles for skin photoprotection through the topical delivery of caffeic acid-phthalimide

Bruna Terra Alves da Silva [a], Sueli de Oliveira Silva Lautenschlager [a,b], Celso Vataru Nakamura [a,b], Valdecir Farias Ximenes [c], Yu Ogawa [d], Raphaël Michel [d,*], Rachel Auzély-Velty [d,*]

[a] Post-Graduate Program in Pharmaceutical Sciences, State University of Maringá, Maringá, Paraná, Brazil
[b] Department of Basic Health Sciences, Maringa State University (UEM), Maringá, Paraná 87020900, Brazil
[c] Department of Chemistry, Faculty of Sciences, São Paulo State University (UNESP), Bauru, São Paulo 17033360, Brazil
[d] Université Grenoble Alpes, CNRS, CERMAV, 38000 Grenoble, France

ARTICLE INFO

*Keywords:*
Caffeic acid-phthalimide
Photoprotection
Solid lipid nanoparticles
Topical delivery

ABSTRACT

Exposure of the skin to ultraviolet (UV) radiation is associated with many pathological conditions such as premature aging and skin cancer. Furthermore, members of Nicotinamide Adenine Dinucleotide Phosphate-oxidase (NADPH oxidase or NOX) enzyme family can produce UV-induced reactive oxygen species (ROS), even after cessation of radiation exposure. The caffeic acid-phthalimide (CF) compound is a potent antioxidant, which reduces the generation of ROS. However, its high lipophilicity may hamper its permeation through the skin. Solid lipid nanoparticles (SLNs) can ensure close contact and increase the amount of drug absorbed into the skin. The present work aims to develop and optimize SLNs containing CF to achieve enhanced skin photoprotection along with antioxidant and anti-aging effects. SLNs were prepared by the hot homogenization method using Compritol 888 ATO as lipid matrix, and Tween 80 and Pluronic® F-127 as surfactants to stabilize the nanoparticle dispersion. The particles had high stability for at least 30 days. Physicochemical characterizations of the selected SLNs formulations showed sizes in the range 150–180 nm, polydispersity index (PDI) of 0.2, and a negative zeta potential ($\cong -25$ mV). The SLNs had high CF entrapment efficiency (96–97 %) and showed a controlled drug-release profile. The *in vitro* study revealed low cytotoxic properties of CF-loaded SLNs towards fibroblasts and a photoprotective effect, reflected from the increased viability of UVB-irradiated fibroblasts treated with CF-SLNs. Moreover, the CF-SLNs induced fibroblast migration and closure, showing that these nanosystems offer not only biological photoprotection, but also stimulate wound healing.

## 1. Introduction

Excessive exposure to ultraviolet (UV) B (290–320 nm) is associated with various skin issues, including premature skin aging and skin cancer, primarily due to the generation of reactive oxygen species (ROS). These ROS not only damage macromolecules like DNA, proteins, and lipids, but also trigger specific signaling pathways that lead to alterations in gene expression (Avadhani et al., 2017). Moreover, UVB induces the activation of ROS-producing NADPH oxidases, which continue to produce the superoxide anion ($O_2^{\bullet}$) even after radiation exposure ceases (Trautinger et al., 2001; Fu et al., 2014; da Silva et al., 2021).

Broad-spectrum organic and inorganic sunscreens are widely used to mitigate the harmful effects of both UVB and UVA (320–400 nm) sunlight radiation (Schneider et al., 2019). However, inorganic molecules such as titanium dioxide and zinc oxide have been associated with skin irritation and photosensitivity, which limits their use (maximum of 25 wt% in sunscreens as mentioned in Bocca et al., 2018; Bordes et al., 2021). This has led to growing interest in biobased organic molecules for photoprotection due to their better tolerability and reduced environmental impact (Ganesan et al., 2016; Petrovic et al., 2023). Naturally occurring polyphenolic acids and their derivatives represent a promising alternative to synthetic sunscreens (Lee et al., 2024). These molecules act as antioxidants by scavenging free radicals and inhibiting the activity and expression of enzymes like NADPH oxidases that generate ROS (dos Santos et al., 2021).

However, phenolic compounds, such as caffeic acid and derivatives,

* Corresponding authors.
*E-mail addresses:* raphael.michel@cermav.cnrs.fr (R. Michel), rachel.auzely@cermav.cnrs.fr (R. Auzély-Velty).

https://doi.org/10.1016/j.ijpharm.2024.125010
Received 18 July 2024; Received in revised form 12 November 2024; Accepted 25 November 2024
Available online 30 November 2024

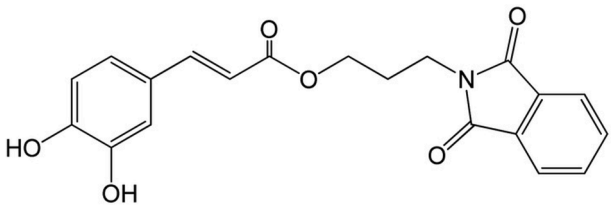


**Fig. 1.** Caffeic acid-phthalimide derivative compound (CF).

are known to be poorly soluble in biological fluids and sensitive to oxidative degradation when exposed to air and light, which can significantly reduce their effectiveness (Figueroa-Robles et al., 2021; Hallan et al., 2021). Therefore, appropriate carriers are required in order to improve their bioavailability, protect them from degradation and ensure the maintenance of their antioxidative power. In that prospect, nanocarrier systems based on natural lipids have attracted significant interest because of their biocompatibility, ability to encapsulate lipophilic molecules, and straightforward production methods that eliminate the need for organic solvents (Mehta et al., 2023; Esposito et al., 2019). Furthermore, lipid-based nanosystems are well-suited for skin applications because their matrix has a strong affinity for the intercellular lipids of the stratum corneum (Esposito et al., 2019). In particular, solid lipid nanoparticles (SLNs) are interesting candidates not only because they were recently used for the oral and topical delivery of phenolic compounds and were shown to offer protection against chemical degradation (Munin et al., 2011; Borges et al., 2020), but also since SLNs can act as physical UV blockers potentialy yielding synergistic protective effect when combined with photoprotective agents (Souto et al., 2020; Netto et al., 2018).

In this context, the present work aims at designing SLNs containing caffeic acid-phthalimide (CF – see formula in Fig. 1) to achieve enhanced skin photoprotection. As reported recently, CF is a potent ROS scavenger and NOX inhibitor (dos Santos et al., 2021). Its ROS scavenging abilities were found slightly lower than those of caffeic acid, but it showed much better capacities as NOX2 inhibitor. To the best of our knowledge, this study reports for the first time the development of an encapsulation strategy for this new antioxidant agent. We systematically investigated formulation parameters that influence the physicochemical characteristics of SLNs, and subsequently evaluated the stability, release profiles of the optimized CF-loaded SLNs, as well as their cytotoxicity and photoprotective properties on fibroblasts.

## 2. Materials and methods

### 2.1. Materials

Compritol 888 ATO was kindly provided by Gattefossé (Saint-Priest, France). Precirol ATO 5 was kindly supplied by Gattefossé (Leon, France). Tween 80 (Polysorbate 80) and Pluronic® F-127 were purchased from Sigma-Aldrich GmbH Merck (Germany). The main characteristics of solid lipids and surfactants used as excipients for SLN development are shown in Table 1. Caffeic acid-phthalimide (370.1 g/mol; RMN spectra are available in SI, Fig. S1) was synthesized by Prof. Valdecir F. Ximenes (Universidade Estadual Paulista UNESP- Bauru) (dos Santos et al., 2021). Water used in all the experiments was purified by using an Elga Purelab purification system, with a resistivity of 18.2 MΩ cm. Amicon® centrifugal filters (ultracel-10 kDa) and dialysis membranes (MWCO 6–8 kDa) were purchased from Sigma-Aldrich GmbH Merck.

### 2.2. Solubility studies for lipid selection

The solubility of CF in different solid lipids was determined by lipid solubility studies (Shah et al., 2007). A fixed amount of drug (10 mg) was weighed accurately and added to 50 mg of lipid melts, namely, Compritol 888 ATO and Precirol ATO 5. The mixtures were maintained under continuous stirring and heated at 10 degrees above the lipid melting point (~70 °C and ~55 °C for Compritol and Precirol, respectively, as reported by Hamdani et al., 2003). The amount of lipid melt was increased by incremental additions of 50 mg until complete solubilization of CF. The formation of a translucent, and homogeneous light brown solution was the endpoint of the solubility study. To verify the stability of CF at elevated temperatures (60–75 °C), UV–Vis absorbance spectra of CF solutions were measured at various temperatures, revealing no significant effects (see Fig. S2).

### 2.3. Formulation procedure

SLN samples were prepared by the hot homogenization method as previously described (Muller et al.., 2004; Manjunath et al., 2005) using a total mass of 4 g for each sample (corresponding to an approximate volume of 4 mL). In a typical preparation protocol, the lipid phase, Compritol 888 ATO and surfactants (Tween 80 or/and Pluronic® F-127) were heated (75 °C) and kept under stirring (magnetic stirrer, 600 rpm, 10–20 min). In the case of CF-loaded samples, caffeic acid-phthalimide was mixed with the lipid phase and kept at a temperature above the solid lipid melting point (75 °C). The hot aqueous phase (ultrapure water) was then added to the melted lipid phase to form a premix. The premix was then subjected to emulsification at 19,000 rpm for 3 min using a T 10 digital Ultra-Turrax® (IKA Works, Inc.). The mixture was further ultrasonicated using a sonicator probe (2 mm diameter; Vibra CellTM, Sonics & Materials Inc., USA), with an amplitude of 70 % for 3 min, at 75 °C. The temperature during the entire process was maintained at 75 °C ± 2 °C. The resulting emulsion was then cooled to room temperature. In the present study, the standard parameters for the preparation of the SLN dispersion were optimized by studying the effect of the emulsification process as well as the influence of the surfactant type and concentration on the mean particle size and dispersity (see section 3.1).

### 2.4. Determination of particle size and polydispersity index

The particle size and polydispersity index (PDI) were measured by dynamic light scattering (DLS) using a Malvern Zetasizer Nano ZS

**Table 1**
Characteristics of solid lipids and surfactants used as excipients for SLNs development.

| Trademark Name | EP Name/USP Name | Chemical Description | Melting Point (∘C) |
|---|---|---|---|
| Compritol 888 ATO | Glycerol dibehenate/Glyceryl dibehenate | Mono-, di-, and triesters of behenic acid ($C_{22}$), the diester fraction being predominant | 65–77 |
| Precirol ATO 5 | Glycerol distearate (type I)/Glyceryl distearate | Esters of palmitic ($C_{16}$) and stearic ($C_{18}$) acids, the diester fraction | 50–60 |
| Tween 80 | Polysorbate 80/Polysorbate 80 | Partial esters of oleic acid with sorbitol and its anhydrides ethoxylated with ethylene oxide (1:20) | −25 |
| Pluronic® F-127 | 2-[2-(2-hydroxyethoxy)propoxy] ethanol | Poly(oxyethylene)-poly(oxypropylene) triblock copolymer | 52–57 |

(Malvern Instruments, UK) at 25 °C. The instrument contains a 4mW He-Ne laser operating at a wavelength of 633 nm. Shortly before each measurement, the nanoparticle dispersions were appropriately diluted (1:1000) with ultrapure water to avoid multiple scattering and shaken manually for a few seconds. During the light scattering experiments, the intensity of the scattered light was recorded at an angle of 173°. The correlation function obtained from the measurement was then analysed with a cumulant fit (i.e. fitting the correlation function with a third order polynomial equation as explained in Koppel, 1972) to extract the average hydrodynamic diameter (referred to as "particle diameter" in this manuscript) and PDI.

### 2.5. Stability assessement

The stability of the SLN formulations was evaluated at room temperature (RT, 25 ± 2 °C) over 30 days. Briefly, all the samples were protected from light and stored in glass vials, analyzed in triplicate and the values of particle diameter and PDI were recorded at different time points (0, 13, 20 and 30 days).

### 2.6. Transmission electron microscopy

The morphology of CF-SLNs was investigated by transmission electron microscopy (TEM) after negative staining as commonly performed on lipid-based nanoparticles (Dora et al., 2012; Benizri et al., 2018). Briefly, one drop of diluted sample (1:50) was placed on a carbon-coated copper grid. After blotting excess liquid, the grid was then stained with a 2 wt% uranyl acetate aqueous solution and allowed to dry in air. The TEM observations were performed using a JEM-2100 Plus (JEOL Japan) operated at 200 kV. The images were recorded on a RIO16 CMOS camera (AMETEK, U.S.A.). Analysis of the SLN diameter was done with the software ImageJ. A minimum of 150 measurements per image were performed.

### 2.7. Release of CF from SLNs

#### 2.7.1. Determination of encapsulation efficiency (EE)

EE (%) values were expressed as the percentage of the entrapped drug compared to the initially added drug. The encapsulation efficiency was herein determined by evaluating the un-encapsulated drug. To achieve this, the CF-loaded SLN (CF-SLNs) formulations were diluted at a ratio of 1:20 in ultrapure water. This dilution was performed to prevent drug crystal deposition on the SLN surface, which could result in inaccurately high EE measurements (Silva et al., 2012). This solution was then centrifuged (9000 rpm for 45 min, 4 °C) in an Amicon® centrifugal filter unit (Ultracel-10 K). By this technique, un-encaspulated drug was recovered in the bottom chamber of the unit (Shah et al., 2014; Sharma et al., 2022). The drug concentration in the bottom chamber was determined by UV/visible spectrophotometry (Bio-Tek®, Power Wave XS) ($\lambda$max = 330 nm) using a calibration curve in the range of 10–100 μg/mL with $r^2 = 0.9998$ (see SI, Fig. S3). EE(%) was calculated mathematically according to the following equation:

$$EE(\%) = \left[\left(W_{initialdrug} - W_{freedrug}\right)/W_{initialdrug}\right] \times 100$$

where $W_{\text{initialdrug}}$ is the mass of drug initially used and $W_{\text{freedrug}}$ is the mass of released drug detected in the lower chamber of the Amicon® filter unit after centrifugation of the SLN formulations.

The drug loading (DL) and the encapsulation capacity (EC) were also calculated from $W_{\text{initialdrug}}$ and $W_{\text{freedrug}}$ using the following equations:

$$DL(\%) = \left[\left(W_{initialdrug} - W_{freedrug}\right)/W_{SLN}\right] \times 100$$

$$EC(\%) = \left[\left(W_{initialdrug} - W_{freedrug}\right)/W_{lipid}\right] \times 100$$

where $W_{\text{SLN}}$ is the total mass of SLN in the system and $W_{\text{lipid}}$ is the total mass of lipid (i.e. Compritol).

#### 2.7.2. In vitro CF release

Cumulative *in vitro* release of CF was carried out by dialysis. For that purpose, 8 mL of the CF-SLNs formulation were placed into a dialysis bag (MWCO 6–8 kDa). The bag was incubated at room temperature in 110 mL of release medium (0.5 % w/v Tween 80 in ultrapure water, pH ≈ 6), (Nazemiyeh et al., 2016). During dialysis, the medium was continuously stirred at 100 rpm with a magnetic stirrer. Samples (2 mL) were collected at specific time intervals (0, 48, 96, 144, 192 and 288 h (=12 days)) and replaced immediately with the same volume of fresh release medium. The concentration of drug released in each collected aliquots was evaluated by measuring its absorbance at 330 nm (Bio-Tek®, Power Wave XS) and comparing it to the calibration curve (see SI, Fig. S3).

The cumulative pourcentage release (%) was calculated as follows:

$$\text{Cumulative percentage release}\,(\%) = \frac{\text{Volume of sample withdrawn}\,(\text{mL})}{\text{Bath volume}\,(\text{V})} \times \text{P(t}-1\text{)} + \text{P(t)}$$

where P(t) is the percentage of drug released at time t and P(t-1) is the percentage of drug released at time t-1.

### 2.8. Cell culture and viability study

The experiments were performed with fibroblast L929 cells (clone NCTC 929, L CELL, L-929; ATCC® CCL1™, Manassas, USA;), provided by Dr. Maria José Vieira Fonseca (Faculty of Pharmaceutical Sciences of Ribeirão Preto, University of São Paulo, Ribeirão Preto, Brazil). Murine fibroblast cells were maintained and cultured in DMEM (DMEM, Life Technologies/Gibco Laboratories, Grand Island, NY, USA) supplemented with 2 mM L-glutamine, 10 % (v/v) fetal bovine serum (FBS, Life Technologies/Gibco Laboratories, Grand Island, NY, USA), penicillin (50 U/mL) and streptomycin (50 μg/mL) at 37 °C in a 5 % $CO_2$ atmosphere. Depending on the experiment, cells were seeded in 96-well plates ($2.5{\cdot}10^5$ cells/mL) or 24-well plates ($2.5{\cdot}10^5$ cells/mL) and maintained in the tissue culture incubator for 24 h to allow monolayer formation.

Cell viability was determined by neutral red assay (3-amino-7-dimethylamino-2-methylphenazine hydrochloride; Inlab®, São Paulo, SP, BR), a cationic dye that stains lysosomes of viable cells (Borenfreund et al., 1985). Cell vability was first evaluated in the absence of UV. For that, L929 fibroblasts in 96-well plates were treated for 24 h with 100 μL SLNs (50 μg/mL) or CF-laden SLNs (0.5–25 μg/mL). Additionally, cell viability was determined after UVB irradiation. In 24-well plates, L929 fibroblasts were treated with 500 μL of CF-SLN (0.5 to 2.5 μg/mL) for 24 h. Subsequently, they were exposed to UVB irradiation (UVB lamp: TL40W/12RS; Philips; peak intensity of 312 nm) applied at an intensity of 600 mJ/cm$^2$ (de Oliveira et al., 2018) monitored using a UV spectra radiometer (VLX-3 W, Vilber Lourmat) and finally incubated for another 24 h. Subsequently, neutral red (40 μg/mL) was added for a period of 3 h. Cells were then fixed with an aqueous solution of formaldehyde (2 % v/v) and calcium chloride (1 % w/v). Immediately following fixation, a solution of acetic acid (1 % v/v) and ethanol (50 % v/v) was added to extract the dye. The readings were taken on a spectrophotometer (Bio-Tek®, Power Wave XS) at 540 nm.

### 2.9. Cell migration

The stimulatory effect of CF-SLNs on the migration of L929 cells was determined as described by Balekar et al., 2012 with some modifications. When the cell monolayer is streaked, it responds to the interruption of cell–cell contacts by increasing the concentration of growth factors and cytokines at the edge of the wound, thus initiating the migration of different types of cells, such as fibroblasts (Liang et al., 2007). To perform this assay, L-929 cells were plated ($2.5{\cdot}10^5$ cells/mL)

in 24-well plates and kept= at 37 °C for 24 h. The next day, cells were incubated with DMEM supplemented with 0.5 % FBS for 6 h. The cell monolayer was wounded in the center of the well with a sterile 20 μL pipette tip, washed with PBS and treated with CF-SLN in supplemented DMEM (0.5 % FBS) at concentrations of 1 and 2.5 μg/mL. Wound healing was observed at times of 0, 24 and 48 h on an inverted phase contrast microscope (Olympus CKX41; 5X magnification). To quantify the open area of the wound, the ImageJ software was used, and the percentage of open wound area was calculated in comparison with the initial wound (at t = 0h).

### 2.10. Statistical analysis

Statistical analyzes were performed using GraphPad Prism software v. 5.00 (San Diego, CA, USA). Tables and graphs show the mean ± standard deviation of at least three independent experiments. Data were analyzed using the ANOVA test (one-way or two-way), followed by Tukey post-test, considering $p \leq 0.05$ as statistically significant.

## 3. Results

### 3.1. Design and optimization of solid lipid nanoparticles

#### 3.1.1. Selection of solid lipid

In order to select the appropriate lipid for the formulation of CF-loaded SLNs, the solubility of CF was tested in two lipids commonly used for SLN formulations, Precirol ATO 5 and Compritol ATO 888. This was done by evaluating the minimum amount of lipid necessary to solubilize 10 mg of CF (see Material and Method section for details). An amount of 200 mg of Compritol was found to be sufficient to solubilize CF, whereas 250 mg of Precirol were required. As CF exhibits a higher solubility in Compritol, this lipid was selected for the preparation of SLNs.

#### 3.1.2. Optimization of the SLN preparation method

In this part, the influence of the preparation method on the characteristics of the SLNs was assessed. To this end, a model formulation of SLN [$4.72{\cdot}10^{-2}$ mol/L (5 wt%) of Compritol and $7.63{\cdot}10^{-3}$ mol/L (1 wt%) of Tween 80 in ultrapure water] was first subjected to 3 different emulsification processes: (i) a single homogenization step with ultra-turrax (19 000 rpm, 3 min, at room temperature), (ii) a single sonication step (70 % of amplitude, 3 min, at 75 °C) and (iii) a combination of both. It can be noted that Tween 80 was chosen as the primary surfactant in this study because it is commonly used in the formulation of SLNs (Makoni et al., 2019; Badawi et al., 2020). Fig. 2-A shows the diameters, measured by DLS, of the SLNs obtained by the different emulsification methods. These results indicate that the lower particle diameter (≈ 290 nm) is obtained by a combination of homogenization and sonication. To further optimize the preparation method, the impact of the sonication time on the SLN size was studied. For that, SLNs [$4.72{\cdot}10^{-2}$ mol/L (5 wt %) of Compritol and $7.63{\cdot}10^{-3}$ mol/L (1 wt%) of Tween in ultrapure water] were prepared by a homogenization step with ultra-turrax (19,000 rpm, 3 min, at room temperature, RT), followed by a sonication step (70 % of amplitude, at 75 °C) of different durations (3, 5 and 7 min). Fig. 2 B displays the particle size and PDI of the resulting SLNs as characterized by DLS. This shows that the SLN characteristics are very similar in the three different samples. The diameters are between 279 and 290 nm and the PDI varies from 0.286 to 0.300, a variation that is below the recorded standard deviation. Hence, the duration of the sonication step does not seem to have an important impact on the SLNs features. Accordingly, a sonication step of 3 min was used to prepare SLNs for the rest of this study.

#### 3.1.3. Optimization of the surfactant concentration

In an attempt to obtain smaller and more monodisperse particles, which are more likely to remain stable for long storage times, we then investigated the effect of the concentration of surfactant on the SLNs

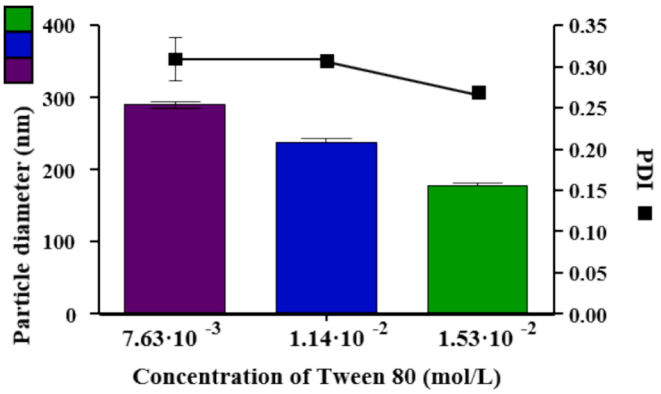


**Fig. 3.** Particle diameter and polydispersity index of SLN formulations containing different Tween 80 concentration: $7.63{\cdot}10^{-3}$ (1 wt%), $1.14{\cdot}10^{-2}$ (1.5 wt %), and $1.53{\cdot}10^{-2}$ mol/L (2 wt%). Error bars correspond to the standard deviation obtained after at least three independent measurements on the same sample.

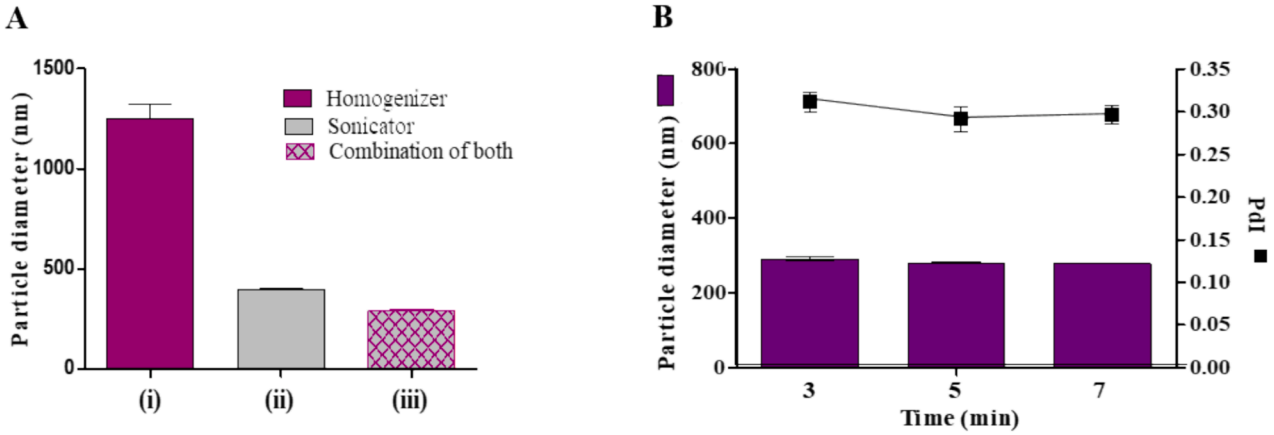


**Fig. 2.** (A) Particle diameter of standard SLNs obtained by different emulsification process methods. (i) a single homogenization step with ultra-turrax (19,000 rpm, 3 min, at room temperature), (ii) a single sonication step (70 % of amplitude, 3 min, at 75 °C) and (iii) a combination of both. (B) Particle Diameter and PDI of standard SLNs prepared with different sonication times (3, 5 and 7 min). The displayed hydrodynamic particle diameter (nm) were obtained by DLS. Error bars correspond to the standard deviation obtained after at least three independent measurements on the same sample.

characteristics. For that, three different formulations of SLNs were prepared with increasing Tween concentration: $7.63{\cdot}10^{-3}$ mol/L (1 wt %); $1.14{\cdot}10^{-2}$ mol/L (1.5 wt%) and $1.53{\cdot}10^{-2}$ mol/L (2 wt%). Fig. 3 shows the diameter and PDI of the resulting SLNs as characterized by DLS. It can be seen that, with increasing Tween concentration, the particle size decreases from 290 to 180 nm (see Fig. 3 A), and the PDI is also reduced from 0.300 to 0.239 (see Fig. 3 B). This is expected as the addition of surfactant reduces the interfacial tension between the lipid and the aqueous phase, thereby allowing the formation of smaller SLNs (and yielding a larger total interfacial area). However, although higher Tween concentrations conveniently lead to smaller particle size, a large quantity of Tween can have a detrimental effect on cells. In fact, studies have shown that for concentrations down to $0.4{\cdot}10^{-3}$ mol/L, Tween 80 exhibits toxicity against human fibroblasts (Arechabala et al., 1999). Accordingly, even though we plan to use our SLN system in diluted conditions for biological assays (up to 5 μg/mL which correspond to a maximum Tween concentration around $4{\cdot}10^{-6}$ mol/L), it is important to limit the surfactant concentration in our formulations.

### 3.1.4. *Effect of surfactant mixture*

One strategy to obtain smaller and more stable SLNs while maintaining the total surfactant concentation is to resort to a mixture of surfactants. In particular, it has been shown that combining Tween 80 with a surfactant displaying a higher hydrophilic/lipophilic balance (HLB), i.e. adding a more hydrophilic surfactant, can yield SLNs of smaller size (Hippalgaonkar et al., 2013; Abdelbary et al., 2009). Accordingly, in this work, Tween 80 (HLB = 15) was combined with Pluronic® F-127 (aslo referred to as Poloxamer 408, HLB = 22). To the best of our knowledge, this precise combination of surfactant was never employed for the formulation of SLNs although Tween 80 was successfully combined with another Poloxamer (Poloxamer 188; HLB = 29) (Hippalgaonkar et al., 2013; Abdelbary et al., 2009). Different molar ratios of surfactants were tested for the preparation of SLNs while maintaining a constant total surfactant concentration as listed in Table 2.

Fig. 4 displays the diameter and PDI of the SLNs obtained with the different mixtures of surfactant. It clearly shows that, as expected, both the diameter and the PDI decrease with increasing Pluronic® content in the mixture. This decrease leads to particle diameters below 200 nm when more than 5 mol% of Pluronic® is used in the surfactant mixture (~150 nm for 10 mol% and ~140 for 15 mol%).

In addition, the colloidal stability of these formulations was investigated over a long storage time. To this aim, DLS measurements were performed on the samples at regular time intervals over a period of 30 days. The resulting data are shown in Fig. 5. It can be seen that the diameter and PDI of the formulations containing Pluronic® F-127 remain stable over 30 days. In contrast, for the formulation based solely on Tween 80, the particle size seems to decrease over time (circular symbols on Fig. 5 A) while there is a concomittant increase of polydispersity (circular symbols on Fig. 5 B). Such an observation could be attributed to the occurrence of aggregation between SLNs in solution. As a matter of fact, the formation of aggregates would enhance the polydispersity whereas the sedimentation of larger aggregates may yield a progressive decrease of the average particle size.

The two formulations containing the most Pluronic® (90:10 and 85:15) will be used in the rest of the manuscript as they lead to small particles (diameter <160 nm) that are stable over time (30 days).

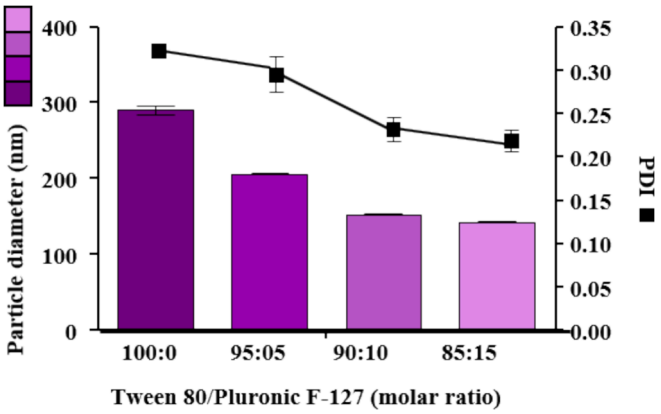


**Fig. 4.** Particle diameter and polydispersity index of SLN formulations containing different molar ratios of the mixture of surfactant Tween 80: Pluronic® F-127 (100:0, 95:05, 90:10 and 85:15). Error bars correspond to the standard deviation obtained after at least three independent measurements on the same sample.

### 3.1.5. *Effect of drug loading on the size and colloidal stability of SLNs*

In the previous sections, the preparation method and the formulation of SLNs were improved in the absence of CF. The aim of this part is to introduce CF in the formulations and investigate its influence on the size and stability of the SLNs.

In that purpose, CF was added to the optimized formulations identified previously (namely the ones containing Tween 80 and Pluronic® F-127 with the ratio 90:10 and 85:15). Two different concentrations of CF were tested: $1.35{\cdot}10^{-5}$ mol/L (2.5 wt% in relation to lipid content) and $2.70{\cdot}10^{-5}$ mol/L (5 wt% in relation to lipid content). Fig. 6 shows the size and polydisperstity of the resulting SLNs shortly after preparation. For both formulations (90:10 and 85:15), the introduction of CF seems to lead to a slight increase in the size of these SLNs. This effect is enhanced when a larger amount of CF is introduced. Comparing the "unloaded" SLNs to the one containing the largest quantity of CF, the diameters expands from 151 to 176 nm (for the formulation 90:10, $2.7{\cdot}10^{-5}$ mol/L) and from 143 to 175 nm (85:15, $2.7{\cdot}10^{-5}$ mol/L). Hence, the addition of CF results in a 20–30 % increase of the SLN diameter which means that the volume of single SLNs increases by 60–85 %. Nevertheless, the size of the CF loaded SLNs remains relatively low (below 200 nm).

Next, the colloidal stability of the CF-loaded SLNs – specifically, their ability to resist particle aggregation – was probed over a 30-day period, following procedures that were used for other colloidal formulations like liposomes (Michel et al., 2013) and nanogels (Abdi et al., 2020). This was done primarily to evaluate the influence of storage time on the CF-loaded SLNs and to establish how long after their preparation the SLNs could still be considered as stable colloidal suspensions. This is crucial for potential commercial applications and, more importantly, for planning the biological assays in the following sections, ensuring that the SLNs remain well-dispersed at the time of the experiments. Accordingly, the hydrodynamic diameter and PDI of SLN formulations stored at room temperature were recorded regularly over 30 days as depicted in Fig. 7. It can be seen on these graphs that the SLNs with the surfactant ratio 85:15 (Tween 80: Pluronic®) have a stable size and PDI over the whole duration of the study. In the case of the formulations with the surfactant ratio 90:10 (Tween 80: Pluronic®), the SLNs containing the largest

**Table 2**
Composition of the prepared SLNs.

| | | | | | |
|---|---|---|---|---|---|
| Compritol ATO 888 concentration | mol/L | $4.72{\cdot}10^{-2}$ | $4.72{\cdot}10^{-2}$ | $4.72{\cdot}10^{-2}$ | $4.72{\cdot}10^{-2}$ |
| Total Surfactant concentration | mol/L | $7.63{\cdot}10^{-3}$ | $7.63{\cdot}10^{-3}$ | $7.63{\cdot}10^{-3}$ | $7.63{\cdot}10^{-3}$ |
| Tween 80 | Molar ratio | 100 | 95 | 90 | 85 |
| Pluronic® F-127 | | 0 | 05 | 10 | 15 |

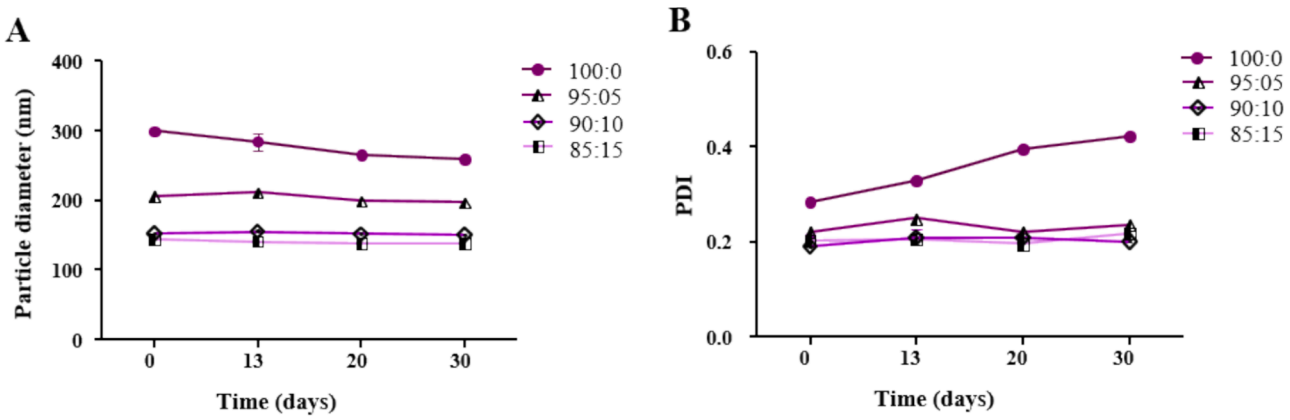


**Fig. 5.** Time dependant measurement of (A) particle diameter and (B) polydispersity index of different SLN formulations containing different molar ratios of the mixture of surfactant Tween 80: Pluronic® F-127 (100:0, 95:05, 90:10 and 85:15). Samples were kept at room temperature (25 ± 4 °C) for the duration of the study. Results were expressed as mean ± SD (n = 3).

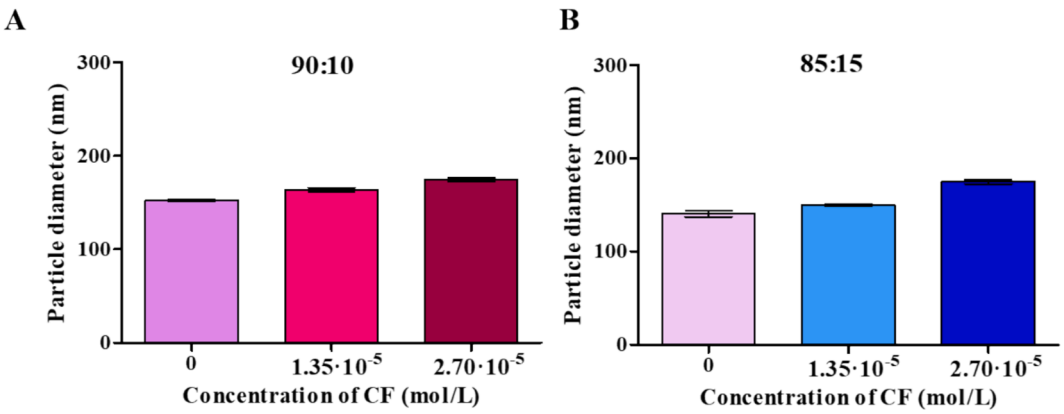


**Fig. 6.** (A) Particle diameter of the 90:10 (pink histogram) and (B) Particle diameter of 85:15 (blue histogram) SLNs. Formulations in the absence (violet histogram) and presence of CF at two different concentrations: $1.35{\cdot}10^{-5}$ mol/L (= 2.5 wt% of total lipid content) and $2.70{\cdot}10^{-5}$ mol/L (= 5 wt% of total lipid content). Error bars correspond to the standard deviation obtained after at least three independent measurements on the same sample.

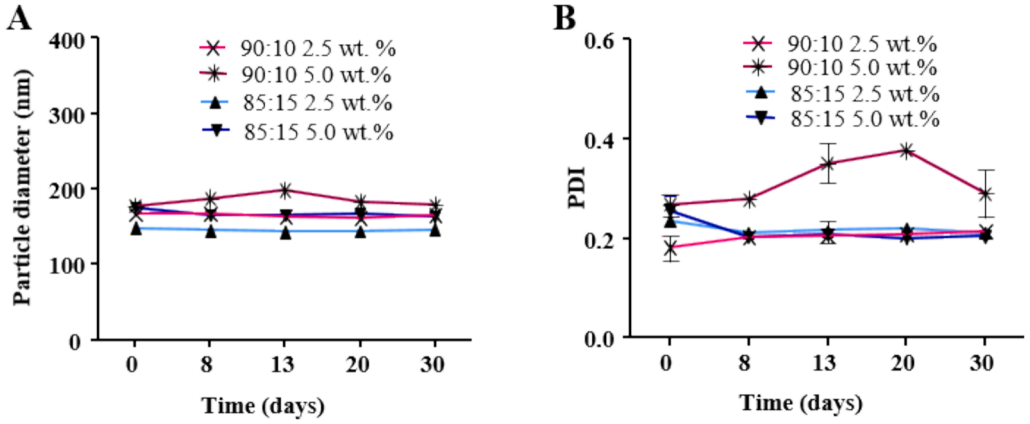


**Fig. 7.** (A) Time dependant measurement of particle diameter and (B) polydispersity index of different SLN formulations containing different mixtures of surfactant Tween 80: Pluronic® F-127 (90:10, and 85:15) as well as different CF concentration (2.5 wt% and 5 wt% in relation to the total mass of lipid). Samples were kept at room temperature (21 ± 4 °C) for the duration of the study. Results were expressed as mean ± SD (n = 3). Error bars correspond to the standard deviation obtained after at least three independent measurements on the same sample.

amount of CF exhibit an increase in size over the first 13 days followed by a size decrease (see Fig. 7 A). This comes along with an important increase in PDI (see Fig. 7 B). As previously seen for unloaded SLNs based on Tween 80 (see Fig. 5, formulation 100:0), such a behavior reveals the instability of the sample and suggests the formation of aggregates of SLNs which are eventually large enough to sediment. On the contrary, for the formulation 90:10 with the lower CF concentration both the size and PDI are stable over time.

To conclude, the design and optimization of SLNs led to the identification of 3 CF-loaded SLN formulations with small diameters

(150–200 nm), reduced polydispersity (PDI ≈ 0.2) and long term colloidal stability (> 30 days). It is worth mentioning that even after 30 days of storage, the size distribution of the SLNs, as measured by DLS (see SI, Fig. S4), showed no evidence of aggregation, with a single particle population observed. This stability can be attributed to the negatively charged surface of the SLNs (as evidenced by a negative Zeta potential, see SI – Fig. S5), which may promote electrostatic repulsion between adjacent particles, thereby delaying the aggregation process.

In the following, the focus will be put on two formulations. First, the SLNs with a surfactant ratio of 85:15 and 5 wt% CF, which contains the largest amount of CF. The second formulation, with a surfactant ratio of 90:10 and 2.5 wt% CF, is selected as an alternative to investigate whether the surfactant composition influences the release efficiency of CF from the SLNs.

It is important to note that, when included in these two SLN formulations, the CF was efficiently protected from photodegradation (as can be seen in SI, Fig. S6).

### 3.2. Microscopic morphology of CF-SLNs

The morphology of the SLNs was investigated by TEM. Fig. 8A shows the micrographs obtained for the formulation 90:10 (2.5 wt%) and 85:15 (5.0 wt%). On these images, SLNs have a polygonal shape. Such an angular morphology was already reported and attributed to lipid crystallization processes (Balamurugan et al., 2018). The particle sizes measured on these images follow a typical log-normal law and the average diameter is 140 nm for the formulation 90:10 and 126 nm for the formulation 85:15 with a large standard deviation (see Fig. 8B). These results are similar to those obtained with DLS data (Fig. 6 and Fig. 7) that feature diameters around 150–170 nm and PDI values above 0.2 (corresponding to a standard deviation of around ± 40 nm).

### 3.3. Release of CF from SLNs

#### 3.3.1. Encapsulation efficiency (EE)

The encapsulation efficiency of 90:10 (2.5 wt%) and 85:15 (5.0 wt%) formulations was determined by separating the un-encapsulated drug by centrifugation using an Amicon tube (Shah et al., 2014; Sharma et al., 2022) and quantifying this "free" drug using UV–visible spectrophotometry (see the Materials and Methods section for details). The results were used to calculate the encapsulation efficiency (EE), drug loading (DL) and encapsulation capacity (EC). The data presented in Table 3 indicate that the CF-SLN formulations with ratios of 90:10 (2.5 wt%) and 85:15 (5.0 wt%) display EE values around 95 %, which are comparable to or exceed those typically reported in the literature for similar SLN formulations (Hippalgaonkar et al., 2013; Abdelbary et al., 2009). The DL values observed in our study are relatively low compared to those typically reported in the literature (ranging from 5 to 10 %, Shah et al., 2014; Hippalgaonkar et al., 2013), suggesting that a greater amount of CF could potentially be incorporated into the SLNs. However, the current loading was considered sufficient to achieve the necessary dose for observing a photoprotective effect.

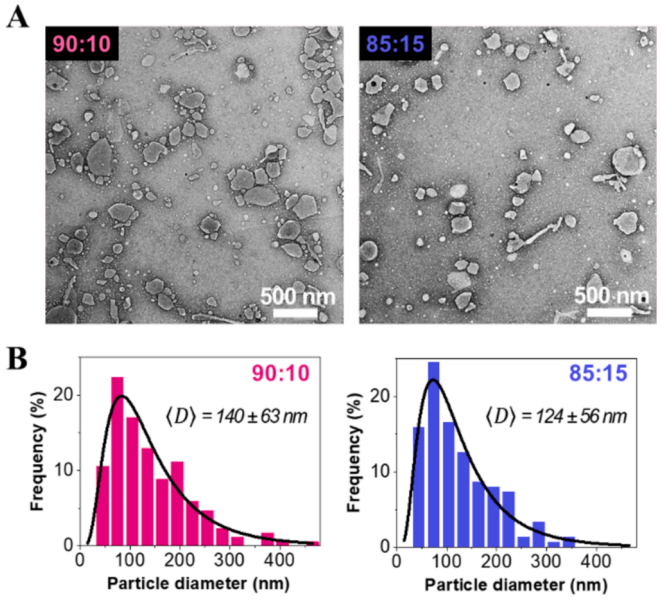


**Fig. 8.** (A) Transmission electron micrographs of CF-SLNs 90:10 (with 2.5 wt% CF) and CF-SLNs 85:15 (with 5.0 wt% CF). (B) Distribution of particle size as measured on TEM images starring the mean diameter (black curves are obtained by fitting the data with a log-normal law).

**Table 3**
Evaluation of the efficiency of encapsulation (EE%), drug loading (DL%) and encapsulation capacity (EC%) of solid lipid nanoparticles (SLN), associated with Caffeic acid-phthalimide (CF-SLNs).

| Formulation | EE% | EC% | DL% |
|---|---|---|---|
| CF-SLNs 90:10 2.5 wt%* | 97 | 2.43 | 1.74 |
| CF-SLNs 85:15 5.0 wt%* | 96 | 4.80 | 3.18 |

* in relation to lipid content.

#### 3.3.2. In vitro controlled release of CF from SLNs

Cumulative *in vitro* release of CF was carried out by the dialysis method in 0.5 % Tween 80 aqueous solution (Nazemiyeh et al., 2016). Fig. 9 shows the cumulative amount of active compound released during 288 h (12 days) from 90:10 SLN- CF 2.5 wt% and 85:15 CF-SLNs 5.0 wt %. The release of CF from both studied systems showed a similar trend, although it appeared to be slightly slower for 85:15 CF-SLNs 5.0 wt%. Throughout the 12 days experiment, the profiles showed sustained release, with 50 % of the total CF amount released after the 12-day time period. These relatively slow and incomplete release may be due to strong interactions between lipid and CF molecules and/or to the mechanism of CF deposition within the particle, leading to a drug-enriched core (Muchow et al., 2008; zur Mühlen et al., 1998). Nevertheless, it should be noted that a CF concentration of only 1 μM is sufficient to decrease total reactive oxygen species in neutrophils and demonstrate antioxidant activity (dos Santos et al., 2021). When the cumulative release percentage was converted to μM, we found that approximately 7 μM was released in 4 h from both formulations. This release could therefore have a significant impact on cells. Finally, a similar *in vitro* release study was conducted under conditions that more closely mimic those of the skin (pH 5, 32 °C, see Fig. S7), resulting in a release profile nearly identical to that shown in Fig. 9.

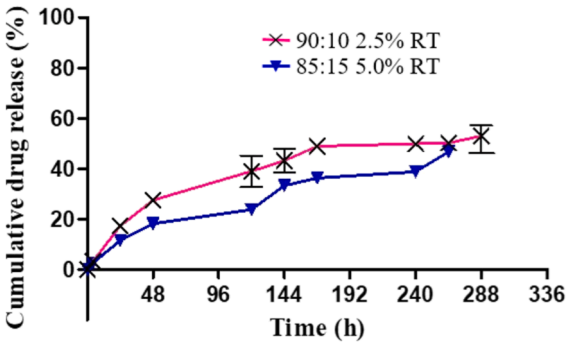


**Fig. 9.** Caffeic acid-phthalimide release profile from SLNs over a period of 288 h.

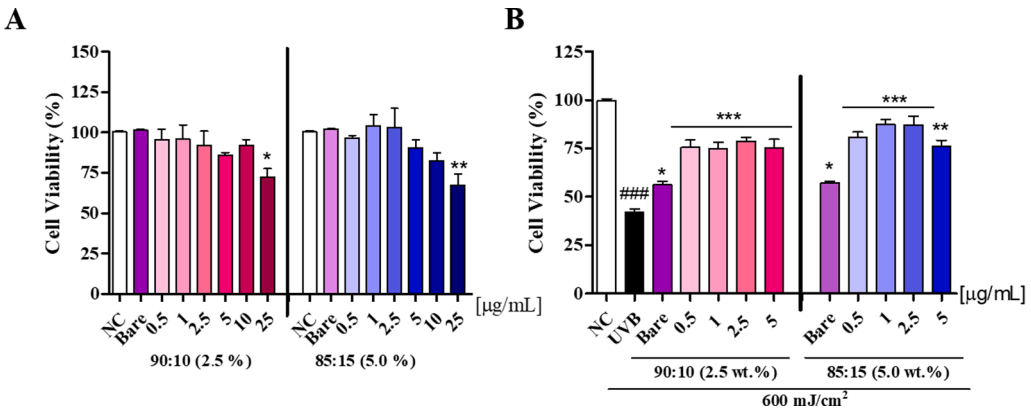


**Fig. 10.** Effect of CF-SLNs 90:10 (2.5 wt%, pink bars) and CF-SLNs 85:15 (5.0 wt%, blue bars) in the (A) cell viability of L929 (B) fibroblasts irradiated with UVB 600 mJ/cm$^2$. Results were expressed as mean ± SD (n = 3). NC: Untreated cells. Bare: SLNs without CF (50 µg/mL). CF-SLNs: 0.5 to 25 µg/mL, 90:10 (pink) and 85:15 (blue). UVB: cells irradiated with UVB (600 mJ/cm$^2$). ###p < 0.001 significant difference compared to NC group. *p ≤ 0.01 and ***p ≤ 0.0001 compared with control.

### 3.4. Viability of L929 fibroblasts in contact with CF-SLNs with and without UVB

For the evaluation of cytotoxic effects of the formulations on skin cells, the viability of L929 cell lines were analyzed after 24 h of treatment with bare SLNs (without CF), or CF-SLNs 90:10 (2.5 wt%) and 85:15 (5.0 wt%) (Fig. 10 A). Bare SLNs (50 µg/mL) and CF-SLNs at lower concentrations (from 0.5 to 10 µg/mL) were nontoxic to fibroblasts,

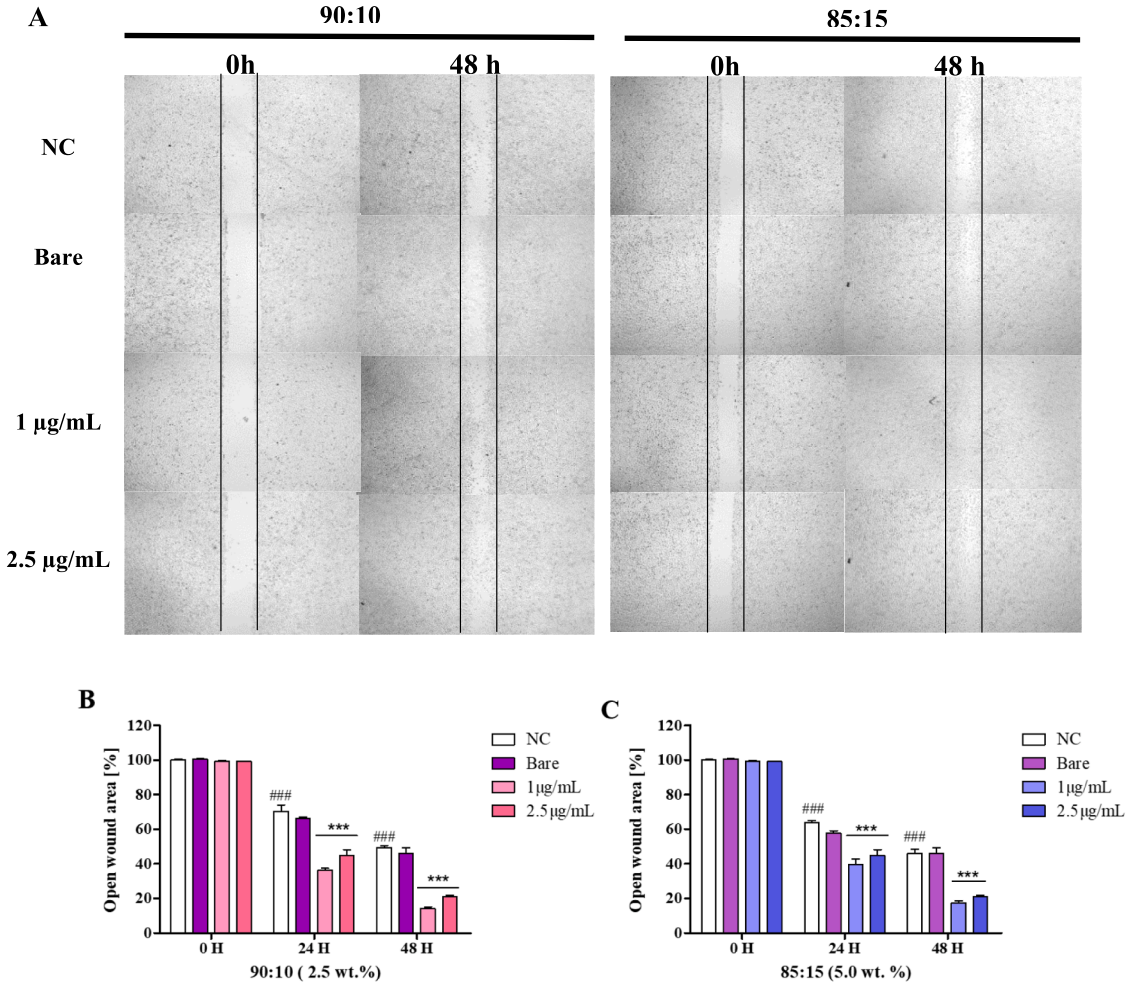


**Fig. 11.** Evaluation of cell migration by the wound healing assay in L929 fibroblasts treated with SLNs for 0 h, 24 h and 48 h. (A) Images were observed under an inverted microscope with phase contrast. (B and C) Images obtained were analysed by ImageJ. NC: negative control; untreated cells. Bare: SLN without CF. CF-SLNs: 1 and 2.5 µg/mL: CF-SLNs 90:10–2.5 wt% (pink bars) and 85:15–5.0 wt% (blue bars). ###p < 0.001, a significant difference compared to CN of 0 h. ***p < 0.001, significant difference compared to 24 h and 48 h NC.

while more concentrated formulation (25 μg/mL) showed cytotoxicity with decreased cell viability by ≅ 27 % compared to NC. We then evaluated the effect of CF-SLNs (90:10 and 85:15) on irradiated fibroblasts (Fig. 10 B). The UVB-irradiated group exhibited a 55 % decrease in viability compared with the untreated cells (NC group). In contrast, fibroblast viability was restored by ≅ 14.08, 33.37 %, 32.77 %, 36.69 % and 33.02 % in the groups treated with bare SLNs (50 μg/mL) and CF-SLNs 90:10 (2.5 wt%) at concentrations of 0.5–5 μg/mL, respectively. And the group treated with bare SLNs (50 μg/mL) and from 0.5 to 5 μg/mL of CF-SLNs 85:15 (5.0 wt%) restored the fibroblast viability in ≅ 14.97 %, 38.64 %, 45.09 %, 44.91 and 33.91 %. Both formulations protected L929 fibroblasts from cell damage caused by UVB radiation.

### 3.5. Impact of CF-SLNs on L929 fibroblast migration

Fibroblast cell migration plays a crucial role in the wound-healing process. To study this migration process, closure of an open wound area, which was created in a cell monolayer, is often investigated (Grada et al., 2017). The scratch wound assay is one of the most highly used *in vitro* methods for probing collective cell migration, and thereby, assessing cell repair rate (Grada et al., 2017; Martinotti et al., 2020). This assay was used for assessing migration of fibroblasts treated with CF-SLNs. Fig. 11 shows that the treatment with CF-SLNs (90:10–2.5 wt% and 85:15–5.0 wt%) at both concentrations (1 and 2.5 μg/mL) at 24 h accelerates L929 cell migration and wound closure by ≅ 61 % and 66 %, respectively (Fig. 11 B and C). At 48 h, treatment with both formulations (90:10–2.5 wt% and 85:15–5.0 wt%) at 1 μg/mL, induced an almost confluent state (87 % and 83 % of wound healing, respectively). At 2.5 μg/mL both formulations increased migration rates by ≅ 80 %. In comparison, the use of bare SLNs (without CF) lead to a wound healing rate very similar to the negative control.

## 4. Discussion

In this work, CF, a photoprotective agent combining antioxidant and NOX inhibitory properties, was successfully formulated in highly biocompatible SLNs to improve its poor stability and bioavailability. SLNs were chosen to ensure CF permeation into deeper layers of the skin and exert the desired cellular photoprotection, since UV radiation reaches all epidermis and dermis layers (Nichols et al., 2010). Various *in vitro* and *in vivo* studies have demonstrated the potential benefits of lipid nanoparticles for skin administration. In addition to enhancing drug penetration into the skin without compromising the skin barrier or causing systemic absorption, lipid nanoparticles offer protection against physical degradation, facilitate controlled drug release, and improve skin moisture and elasticity. (Chen-yu et al., 2012; Gupta et al., 2012; Vitorino et al., 2014).

The formulation of SLNs (lipid, surfactant composition, and CF content) and their preparation method were investigated and optimized to obtain SLNs of suitable size for topical applications. The optimal particle size generally ranges from 100 to 400 nm (Xu et al., 2022), which ensures both effective application and long-term colloidal stability. Smaller particles, such as those with sizes of 140 nm (for the 90:10 formulation) and 126 nm (for the 85:15 formulation), are inherently less prone to aggregation and sedimentation which extends their shelf life and facilitates storage. We selected Compritol 888 ATO as the solid lipid core for encapsulating CF based on the solubility of CF in molten lipids. The influence of the preparation methods on the characteristics of the SLNs was first assessed and it was found that SLNs obtained by a combination of homogenization and sonication exhibited sizes in the targeted range (100–400 nm). This result was consistent with previous studies (Pandey et al., 2020) which showed that a high amount of energy is necessary to achieve the proper dispersion of SLNs. Accordingly, homogenization and sonication were used to prepare SLNs in the rest of this work.

The surfactants chosen to stabilize the structure of SLNs were Tween 80 and Pluronic® F-127. Using a combination of two surfactants, rather than just one, proved more effective in reducing the interfacial tension of nanoparticles, preventing aggregation, and resulting in smaller, more stable nanoparticles. Such strategy was used in several other investigations with other surfactant combinations (Tan et al., 2010; Rawat, et al., 2010; Hippalgaonkar et al., 2013; Abdelbary et al., 2009).

The SLNs with Tween 80:Pluronic® F-127 ratios of 90:10 and 85:15 showed a high encapsulation efficiency (>95 %) in both formulations. The high lipophilicity of CF likely favors the interactions of the compound with the lipids. A valuable next step for this study would be to gather data on the physical state of CF following its incorporation into SLNs, which could provide deeper insights into CF-lipids interactions.

Then, the physicochemical stability of the formulations was evaluated at room temperature over 30 days. The 90:10 formulation with 2.5 wt% of CF and the 85:15 formulation with 2.5 wt% and 5 wt% of CF display high colloidal stability over a period of 30 days (see Fig. 7). This characteristic is crucial for potential commercial applications requiring a prolonged shelf life. It also ensures that the SLNs remain well-dispersed over the time necessary to perform the biological assays presented in the rest of the manuscript. The resistance of our SLNs to aggregation can be attributed to the combination of steric stabilization provided by the non-ionic surfactants and repulsive electrostatic interaction between the negatively charged surface of SLNs, as indicated by a negative Zeta potential (see Fig. S5). However, the observation of a negative surface potential is surprising, considering that both surfactants used (Tween 80 and Pluronic F-127) are non-ionic. In the present case, the negative charge is likely due to slight ionization of glyceryl behenate, a fatty acid in Compritol. Such an effect has been reported in the literature several times (Khan et al., 2018; Eleraky et al., 2020).

The *in vitro* release study showed a slow and progressive release of CF from both formulations (90:10 and 85:15) over a period of 12 days (monitored period). This release rate correponds to an increase of CF concentration of ~1.5 to 2 μM/hour. Interestingly, at such concentrations, CF is known to have a significant effect on cells (dos Santos et al., 2021). Hence such release profile may well be suitable to induce photoprotection.

To prove this hypothesis, we showed that CF-SLNs 90:10 and 85:15 are not cytotoxic at low concentrations and restored cell viability after UVB-induced cytotoxicity. UVB (290–320 nm) reaches the epidermis and the upper layer of the dermis leading to photoaging processes in fibroblasts cells, present on the dermis, as well. In addition, incorporating CF into SLNs for topical photoprotection proved beneficial, as it enhanced photostability of CF by protecting it from physical degradation under UVB radiation (see Fig. S6).

Moreover, CF-SLNs promoted fibroblast migration and wound healing. This confirms that CF was released in sufficient amounts to protect the cells from UVB-induced damage and to promote wound healing. As such, our CF-SLN design is an interesting candidate for photoprotective formulations. Our findings highlight the need for additional studies on skin permeation and penetration to confirm the feasibility of delivering CF into the upper layers of the skin via topical application of CF-loaded SLNs with minimal toxicity effects (Daré et al., 2020).

## 5. Conclusion

In conclusion, SLNs containing CF as a photoprotective agent were successfully developed by using a hot homogenization process coupled with sonication. Three physical stable CF-SLNs formulations with diameters below 200 nm and high encapsulation efficiency were obtained. The SLNs with different CF concentrations and surfactant compositions exhibited sustained release properties, and low cytotoxicity towards L929 fibroblasts. In addition, they proved to provide effective photoprotection of fibroblasts against UV-irradiation and stimulated wound healing. Thus, our CF-loaded SLNs are promising candidates for topical photoprotective strategy against UV-induced skin photodamage and photoaging.

## CRediT authorship contribution statement

**Bruna Terra Alves da Silva:** Investigation, Writing – original draft, Validation – review & editing. **Sueli de Oliveira Silva Lautenschlager:** Methodology, Data curation, Conceptualization, Writing – review & editing, Supervision, Resources. **Celso Vataru Nakamura:** Conceptualization, Supervision, Resources, Funding acquisition, Validation, Writing – review & editing. **Valdecir Farias Ximenes:** Methodology, Conceptualization, Validation, Writing – review & editing. **Yu Ogawa:** Investigation, Validation, Writing – review & editing. **Raphaël Michel:** Writing – original draft, Writing – review & editing, Visualization, Validation, Supervision, Methodology, Formal analysis, Data curation, Conceptualization. **Rachel Auzély-Velty:** Writing – original draft, Writing – review & editing, Conceptualization, Visualization, Validation, Supervision, Resources, Project administration, Funding acquisition. All authors discussed and revised the paper.

## Declaration of competing interest

The authors declare that they have no known competing financial interests or personal relationships that could have appeared to influence the work reported in this paper.

## Acknowledgment

The authors gratefully acknowledge CAPES/COFECUB program (Ph-C 911/18) for financial support and for scholarship provided to B. T. A. S. They also thank Conselho Nacional de Desenvolvimento Científico e Tecnológico (CNPq), Fundação Araucária, and Complexo de Centrais de Apoio à Pesquisa (COMCAP) - Universidade Estadual de Maringá for financial support.

## Appendix A. Supplementary material

Supplementary data to this article can be found online at https://doi.org/10.1016/j.ijpharm.2024.125010.

## Data availability

Data will be made available on request.

## References

Abdelbary, G., Fahmy, R.H., 2009. Diazepam-loaded solid lipid nanoparticles: design and characterization. AAPS PharmSciTech 10, 211–219.
Abdi, F., Michel, R., Poirot, R., Dakir, M., Sancey, L., Ravaine, V., Auzély-Velty, R., 2020. Dynamic covalent chemistry enables reconfigurable all-polysaccharide nanogels. Macromol. Rapid Commun. 41 (15), 2000213.
Arechabala, B., Coiffard, C., Rivalland, P., Coiffard, L.J.M., Roeck-Holtzhauer, Y.D., 1999. Comparison of cytotoxicity of various surfactants tested on normal human fibroblast cultures using the neutral red test, MTT assay and LDH release. J. Appl. Toxicol. 19 (3), 163–165.
Avadhani, K.S., Manikkath, J., Tiwari, M., Chandrasekhar, M., Godavarthi, A., Vidya, S. M., Hariharapura, R.C., Kalthur, G., Udupa, N., Mutalik, S., 2017. Skin delivery of epigallocatechin-3-gallate (EGCG) and hyaluronic acid loaded nano-transfersomes for antioxidant and anti-aging effects in UV radiation induced skin damage. Drug Deliv. 24 (1), 61–74.
Badawi, N., El-Say, K., Attia, D., El-Nabarawi, M., Elmazar, M., Teaima, M., 2020. Development of pomegranate extract-loaded solid lipid nanoparticles: quality by design approach to screen the variables affecting the quality attributes and characterization. ACS Omega 5 (34), 21712–21721.
Balamurugan, K., Chintamani, P., 2018. Lipid nano particulate drug delivery: An overview of the emerging trend. Pharma Innov. J 7, 779–789.
Balekar, N., Katkam, N.G., Nakpheng, T., Jehtae, K., Srichana, T., 2012. Evaluation of the wound healing potential of Wedelia trilobata (L.) leaves. J. Ethnopharmacol. 141 (3), 817–824.
Benizri, S., Ferey, L., Alies, B., Mebarek, N., Vacher, G., Appavoo, A., Staedel, C., Gaudin, K., Barthélémy, P., 2018. Nucleoside-lipid-based nanocarriers for sorafenib delivery. Nanoscale Res. Lett. 13 (1), 17.
Bocca, B., Caimi, S., Senofonte, O., Alimonti, A., Petrucci, F., 2018. ICP-MS based methods to characterize nanoparticles of $TiO_2$ and ZnO in sunscreens with focus on regulatory and safety issues. Sci. Total Environ. 630, 922–930.
Bordes, C., Bolzinger, M.-A., El Achak, M., Pirot, F., Arquier, D., Agusti, G., Chevalier, Y., 2021. Formulation of Pickering emulsions for the development of surfactant-free sunscreen creams. Int. J. Cosmet. Sci. 43 (4), 432–445.
Borenfreund, E., Puerner, J.A., 1985. A simple quantitative procedure using monolayer cultures for cytotoxicity assays (HTD/NR-90). J. Tissue Cult. Methods 9, 7–9.
Borges, A., de Freitas, V., Mateus, N., Fernandes, I., Oliveira, J., 2020. Solid lipid nanoparticles as carriers of natural phenolic compounds. Antioxidants 9 (10).
Chen-yu, G., Chun-fen, Y., Qi-lu, L., Qi, T., Yan-wei, X., Wei-na, L., Guang-Xi, Z., 2012. Development of a quercetin-loaded nanostructured lipid carrier formulation for topical delivery. Int. J. Pharm. 430 (1–2), 292–298.
da Silva, B.T.A., Peloi, K.E., Ximenes, V.F., Nakamura, C.V., Lautenschlager, S.D.O.S., 2021. 2-acetylphenothiazine protects L929 fibroblasts against UVB-induced oxidative damage. J. Photochem. Photobiol. B Biol. 216, 112130.
Daré, R.G., Costa, A., Nakamura, C.V., Truiti, M.C.T., Ximenes, V.F., Lautenschlager, S.O. S., Sarmento, B., 2020. Evaluation of lipid nanoparticles for topical delivery of protocatechuic acid and ethyl protocatechuate as a new photoprotection strategy. Int. J. Pharm. 582, 119336.
de Oliveira, M.M., Daré, R.G., Barizão, É.O., Visentainer, J.V., Romagnolo, M.B., Nakamura, C.V., Truiti, M.D.C.T., 2018. Photodamage attenuating potential of Nectandra hihua against UVB-induced oxidative stress in L929 fibroblasts. J. Photochem. Photobiol. B Biol. 181, 127–133.
Dora, C.L., Putaux, J.L., Pignot-Paintrand, I., Dubreuil, F., Soldi, V., Borsali, R., Lemos-Senna, E., 2012. Physicochemical and morphological characterizations of glyceryl tristearate/castor oil nanocarriers prepared by the solvent diffusion method. J. Braz. Chem. Soc. 23, 1972–1981.
Dos Santos, W.H., Yoguim, M.I., Daré, R.G., da Silva-Filho, L.C., Lautenschlager, S.O.S., Ximenes, V.F., 2021. Development of a caffeic acid–phthalimide hybrid compound for NADPH oxidase inhibition. RSC Adv. 11 (29), 17880–17890.
Eleraky, N.E., Omar, M.M., Mahmoud, H.A., Abou-Taleb, H.A., 2020. Nanostructured lipid carriers to mediate brain delivery of temazepam: design and in vivo study. Pharmaceutics 12 (5).
Esposito, E., Sguizzato, M., Drechsler, M., Mariani, P., Carducci, F., Nastruzzi, C., Valacchi, G., Cortesi, R., 2019. Lipid nanostructures for antioxidant delivery: a comparative preformulation study. Beilstein J. Nanotechnol. 10, 1789–1801.
Figueroa-Robles, A., Antunes-Ricardo, M., Guajardo-Flores, D., 2021. Encapsulation of phenolic compounds with liposomal improvement in the cosmetic industry. Int. J. Pharm. 593, 120125.
Fu, X.J., Peng, Y.B., Hu, Y.P., Shi, Y.Z., Yao, M., Zhang, X., 2014. NADPH oxidase 1 and its derived reactive oxygen species mediated tissue injury and repair. Oxidat. Med. Cell. Long.
Ganesan, P., Choi, D.-K., 2016. Current application of phytocompound-based nanocosmeceuticals for beauty and skin therapy. Int. J. Nanomed. 11, 1987–2007.
Grada, A., Otero-Vinas, M., Prieto-Castrillo, F., Obagi, Z., Falanga, V., 2017. Research techniques made simple: analysis of collective cell migration using the wound healing assay. J. Invest. Dermatol. 137 (2), e11–e16.
Gupta, M., Vyas, S.P., 2012. Development, characterization and in vivo assessment of effective lipidic nanoparticles for dermal delivery of fluconazole against cutaneous candidiasis. Chem. Phys. Lipids 165 (4), 454–461.
Hallan, S.S., Sguizzato, M., Drechsler, M., Mariani, P., Montesi, L., Cortesi, R., Björklund, S., Ruzgas, T., Esposito, E., 2021. The potential of caffeic acid lipid nanoparticulate systems for skin application: in vitro assays to assess delivery and antioxidant effect. Nanomaterials 11 (1).
Hamdani, J., Moës, A.J., Amighi, K., 2003. Physical and thermal characterisation of Precirol® and Compritol® as lipophilic glycerides used for the preparation of controlled-release matrix pellets. Int. J. Pharm. 260 (1), 47–57.
Hippalgaonkar, K., Adelli, G.R., Hippalgaonkar, K., Repka, M.A., Majumdar, S., 2013. Indomethacin-loaded solid lipid nanoparticles for ocular delivery: development, characterization, and in vitro evaluation. J. Ocul. Pharmacol. Ther. 29 (2), 216–228.
Khan, A.A., Abdulbaqi, I.M., Abou Assi, R., Murugaiyah, V., Darwis, Y., 2018. Lyophilized hybrid nanostructured lipid carriers to enhance the cellular uptake of verapamil: statistical optimization and in vitro evaluation. Nanoscale Res. Lett. 13 (1), 323.
Koppel, D.E., 1972. Analysis of macromolecular polydispersity in intensity correlation spectroscopy: the method of cumulants. J. Chem. Phys. 57 (11), 4814–4820.
Lee, S.J., Lee, D., Park, S.A., Park, J.J., Park, W.H., 2024. Hyaluronic acid/polyphenol sunscreens with broad-spectrum UV protection properties from tannic acid and quercetin. Int. J. Biol. Macromol. 257, 128585.
Liang, C.C., Park, A.Y., Guan, J.L., 2007. In vitro scratch assay: a convenient and inexpensive method for analysis of cell migration in vitro. Nat. Protoc. 2 (2), 329–333.
Makoni, P.A., Wa Kasongo, K., Walker, R.B., 2019. Short term stability testing of efavirenz-loaded solid lipid nanoparticle (SLN) and nanostructured lipid carrier (NLC) dispersions. Pharmaceutics 11 (8).
Manjunath, K., Reddy, J.S., Venkateswarlu, V., 2005. Solid lipid nanoparticles as drug delivery systems. Methods Find Exp. Clin. Pharmacol. 27 (2), 127–144.
Martinotti, S., Ranzato, E., 2020. Scratch wound healing assay. Epidermal cells: methods and protocols 225–229.
Mehta, M., Bui, T.A., Yang, X., Aksoy, Y., Goldys, E.M., Deng, W., 2023. Lipid-based nanoparticles for drug/gene delivery: an overview of the production techniques and difficulties encountered in their industrial development. ACS Mater. Au 3 (6), 600–619.
Michel, R., Plostica, T., Abezgauz, L., Danino, D., Gradzielski, M., 2013. Control of the stability and structure of liposomes by means of nanoparticles. Soft. Matter. 9 (16), 4167–4177.

Muchow, M., Maincent, P., Müller, R.H., 2008. Lipid nanoparticles with a solid matrix (SLN®, NLC®, LDC®) for oral drug delivery. Drug Dev. Ind. Pharm. 34 (12), 1394–1405.
Muller, R.H., Keck, C.M., 2004. Challenges and solutions for the delivery of biotech drugs–a review of drug nanocrystal technology and lipid nanoparticles. J. Biotechnol. 113 (1–3), 151–170.
Munin, A., Edwards-Lévy, F., 2011. Encapsulation of natural polyphenolic compounds; a review. Pharmaceutics 3 (4), 793–829.
Nazemiyeh, E., Eskandani, M., Sheikhloie, H., Nazemiyeh, H., 2016. Formulation and physicochemical characterization of lycopene-loaded solid lipid nanoparticles. Adv. Pharm. Bull. 6 (2), 235–241.
Netto MPharm, G., Jose, J., 2018. Development, characterization, and evaluation of sunscreen cream containing solid lipid nanoparticles of silymarin. J. Cosmet. Dermatol. 17 (6), 1073–1083.
Nichols, J.A., Katiyar, S.K., 2010. Skin photoprotection by natural polyphenols: anti-inflammatory, antioxidant and DNA repair mechanisms. Arch. Dermatol. Res. 302 (2), 71–83.
Pandey, A., 2020. Solid lipid nanoparticles: a multidimensional drug delivery system. Nanosci. Med. 1, 249–295.
Petrovic, S.M., Barbinta-Patrascu, M.-E., 2023. Organic and biogenic nanocarriers as bio-friendly systems for bioactive compounds' delivery: state-of-the art and challenges. Materials 16 (24).
Rawat, M.K., Jain, A., Mishra, A., Muthu, M.S., Singh, S., 2010. Development of repaglinide loaded solid lipid nanocarrier: selection of fabrication method. Curr. Drug Deliv. 7 (1), 44–50.
Schneider, S.L., Lim, H.W., 2019. A review of inorganic UV filters zinc oxide and titanium dioxide. Photodermatol. Photoimmunol. Photomed. 35 (6), 442–446.
Shah, K.A., Date, A.A., Joshi, M.D., Patravale, V.B., 2007. Solid lipid nanoparticles (SLN) of tretinoin: Potential in topical delivery. Int. J. Pharm. 345 (1), 163–171.
Shah, R.M., Malherbe, F., Eldridge, D., Palombo, E.A., Harding, I.H., 2014. Physicochemical characterization of solid lipid nanoparticles (SLNs) prepared by a novel microemulsion technique. J. Colloid Interf. Sci. 428, 286–294.
Sharma, A.N., Upadhyay, P.K., Dewangan, H.K., 2022. Development, evaluation, pharmacokinetic and biodistribution estimation of resveratrol-loaded solid lipid nanoparticles for prostate cancer targeting. J. Microencapsul. 39 (6), 563–574.
Silva, A.C., Kumar, A., Wild, W., Ferreira, D., Santos, D., Forbes, B., 2012. Long-term stability, biocompatibility and oral delivery potential of risperidone-loaded solid lipid nanoparticles. Int. J. Pharm. 436 (1), 798–805.
Souto, E.B., Baldim, I., Oliveira, W.P., Rao, R., Yadav, N., Gama, F.M., Mahant, S., 2020. SLN and NLC for topical, dermal, and transdermal drug delivery. Expert Opin. Drug Deliv. 17 (3), 357–377.
Tan, S.W., Billa, N., Roberts, C.R., Burley, J.C., 2010. Surfactant effects on the physical characteristics of Amphotericin B-containing nanostructured lipid carriers. Colloids Surf. A Physicochem. Eng. Asp. 372 (1–3), 73–79.
Trautinger, F., 2001. Mechanisms of photodamage of the skin and its functional consequences for skin ageing. Clin. Exp. Dermatol. 26 (7), 573–577.
Vitorino, C., Almeida, A., Sousa, J., Lamarche, I., Gobin, P., Marchand, S., Pais, A., 2014. Passive and active strategies for transdermal delivery using co-encapsulating nanostructured lipid carriers: in vitro vs. in vivo studies. Eur. J. Pharm. Biopharm. 86 (2), 133–144.
Xu, L., Wang, X., Liu, Y., Yang, G., Falconer, R.J., Zhao, C.X., 2022. Lipid nanoparticles for drug delivery. Adv. NanoBiomed. Res. 2 (2), 2100109.
zur Mühlen, A., Schwarz, C., Mehnert, W., 1998. Solid lipid nanoparticles (SLN) for controlled drug delivery – Drug release and release mechanism. Eur. J. Pharm. Biopharm. 45 (2), 149–155.